The Use of Surface-Elastic-Wave Reflection Gratings in Large Time–Bandwidth Pulse-Compression Filters

RICHARD C. WILLIAMSON AND HENRY I. SMITH

Invited Paper

Abstract—A new type of surface-wave device has been developed which uses the reflection of surface elastic waves to achieve a desired transfer function. A series of experiments on the reflection of surface waves at normal and oblique incidence from periodic arrays of grooves and overlayer stripes provided guidelines for the choice of the type of reflector, the reflection angle, and the depth of grooves. A prototype pulse-compression filter with a time–bandwidth product of 1500 ($T=30$ μs, $\Delta f=50$ MHz) has been developed. The grooves were etched into $LiNbO_3$ by a neutralized argon ion beam in a manner which provided precise depth control and a desired amplitude response. This reflective-array compressor (RAC) has proved to be relatively free of spurious signals and second-order effects and, as a result, large capacities have been obtained. In the prototype device, rms phase errors were 3.5 deg or less and, as a result, the compressed-pulse sidelobe structure was near ideal. A compression ratio of 1500 was demonstrated. The same device, when operated over a wider bandwidth, yielded a compression ratio of about 4000 with only a modest sacrifice in the level of the time sidelobes.

I. Introduction

SURFACE ELASTIC WAVES have been successfully employed in a number of signal-processing devices, such as delay lines, bandpass filters, phase-coded matched filters, and dispersive delay lines for use as pulse compressors in radar systems [1]–[5]. In almost all cases, piezoelectric substrates have been used, and a desired transfer function obtained by adjusting the form and placement of the electrodes in an interdigital transducer. The design and analysis procedures for such devices are well developed and, as evidence of this, surface-wave devices have become widely used in a number of communications and radar applications. However, interdigital-electrode transducers give rise to a number of undesirable side effects, such as wavefront distortion, multiple reflections, reradiation, bulk-wave generation, dispersion, and variation of effective surface-wave velocity across the array [5]–[7]. These lead to spurious signals, and design procedures to minimize transfer-function errors have become more complex as device capacities have increased. In view of this, we sought an alternate means of high-capacity signal processing which might be relatively free of spurious effects.

Sittig and Coquin [8] noted that reflections of elastic waves from gratings in a strip or on a surface could be used to implement pulse compression and other types of filter functions. However, initial tests in strip-shear and surface-wave configurations proved unsatisfactory [8], [9] and, with one major exception, this line of development has been ignored. The exception, which is described elsewhere in this issue, is a device known as IMCON [9]. It was developed by T. Martin and uses the reflection of the lowest SH plate mode from symmetrical arrays of oblique grooves ("chevron" or "herring bone" patterns) in the surface of a strip delay line to achieve large time–bandwidth pulse compression with low spurious signals.

Manuscript received September 29, 1972; revised November 22, 1972. This work was sponsored by the Department of the Army.

The authors are with the Massachusetts Institute of Technology, Lincoln Laboratory, Lexington, Mass. 02173.

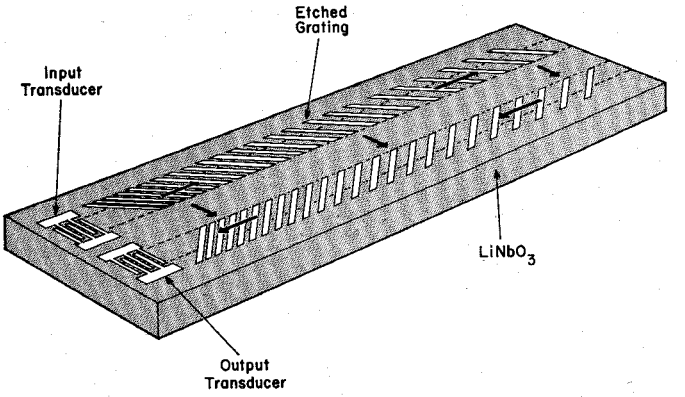

Fig. 1. Schematic diagram of the RAC. Propagation paths at different frequencies are indicated.

As the frequency of operation of IMCON is increased, the thickness of the strip must be reduced. Practical limitations on how thin a strip can be made lead to severe bandwidth restrictions. With this in mind, yet prompted by the excellent results achieved with IMCON devices, we embarked upon a program to develop a similar device using surface waves. We call such a device a reflective-array compressor (RAC). Although this paper will concentrate on the development and performance of this large time–bandwidth pulse compressor, reflective gratings have far wider applications, and many of the comments contained herein can be applied to the more general category of surface-wave reflective-array filters. One such application is in narrow band filters, as reported by Melngailis *et al.* [10].

Our initial goal was to build a prototype RAC for linear FM pulse compression having a time–bandwidth product in excess of 1500 ($T=30$ μs, $\Delta f=50$ MHz). This goal was met by the device shown schematically in Fig. 1. A surface wave is launched in the Z direction on the Y-face of lithium niobate by the interdigital-electrode input transducer. This wave travels through an oblique grating consisting of 6000 grooves whose spacing increases as a function of distance from the input transducer. The surface wave is strongly reflected at a right angle in a region where the groove spacing in the Z direction matches the wavelength of the surface wave. A second reflection in the symmetrically placed mirror-image grating sends the wave to the output transducer. The groove positions are established such that the surface wave travels from input to output along a path whose length (and delay) is linearly

related to frequency. The RAC has proven to be relatively free of second-order effects and, as a result, large capacities have been obtained. Preliminary results have been reported elsewhere [11].

In this paper, we will first describe a number of experiments on surface-wave reflections from gratings which were necessary in order to establish guidelines for the design of RAC and other types of reflective-array devices. These experiments enabled us to make choices of the substrate material and orientation, the type of reflector (overlayer or groove), the reflector angle, the reflectivity of each line in the grating, the position and width of reflecting lines, the acoustic beamwidth, and the forms of the input and output transducers. The reasons behind these design choices and the background experiments are described in Section II. Following that, the fabrication and testing of the prototype RAC are described in Sections III and IV.

II. Background Experiments

Lithium niobate was chosen as the substrate material because it has relatively high piezoelectric coupling, relatively low acoustic loss, and is readily available from commercial sources. We chose to launch and receive surface waves in the Z direction on the Y-face because such waves exhibit low diffraction loss and high coupling efficiency. The prototype RAC device and all the experiments described in this section used Y-cut $LiNbO_3$.

A. Reflection at Normal Incidence from Periodic Gratings

A series of experiments were carried out in which surface waves were reflected at normal incidence from periodic gratings [12] in order to answer the following questions. What sort of reflector is preferred? How can reflectivity be varied? How is the velocity of a surface wave altered as it travels through a grating? The configuration of these experiments is shown in Fig. 2. A surface wave launched by the input transducer traveled under the tap transducer which measured the relative amplitudes of the incident wave and the wave reflected from the grating. The third transducer monitored the transmission through the grating. The grating consisted of 50 or 100 lines of 2.5-μm width on 5-μm centers .Peak reflections occurred at approximately 343 MHz.

We measured the performance of two kinds of reflectors: Nonconducting overlayer stripes and sputter-etched grooves. The overlayer stripes were electron-beam evaporated SiO. These and the sputter-etched grooves exhibited excellent reflection characteristics. The sputter-etched grooves, however, have a number of special advantages. Their use avoids possible problems of adhesion, variations of mechanical properties, acoustic loss, and dispersion associated with deposited overlayers. In the early stages of our work, it was not clear that the reflectivity of sputter-etched grooves could be precisely controlled. As will be described below, this problem was solved, and, as a result, the study of overlayer gratings was terminated and etched grooves were extensively characterized and employed in the prototype RAC. However, overlayer stripes may have considerable utility in some types of reflective-array devices.

The normal-incidence experiments yielded data on the transmission and reflection coefficients of the gratings as a function of frequency and groove depth. These measurements were analyzed on the basis of the model of Sittig and Coquin [8] in order to determine the dependence of the reflectivity of a single step on its height. This dependence is shown in Fig. 3.

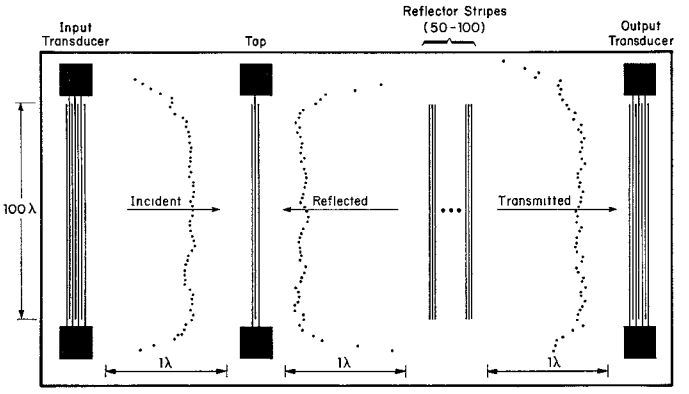

Fig. 2. Experimental configuration for tests of the reflection of surface waves from a periodic grating at normal incidence. The center tap transducer measures the relative amplitudes of the incident and reflected waves. The insets show the wavefronts of the incident, reflected, and transmitted waves plotted on an expanded horizontal scale where the distance corresponding to an acoustic wavelength is indicated.

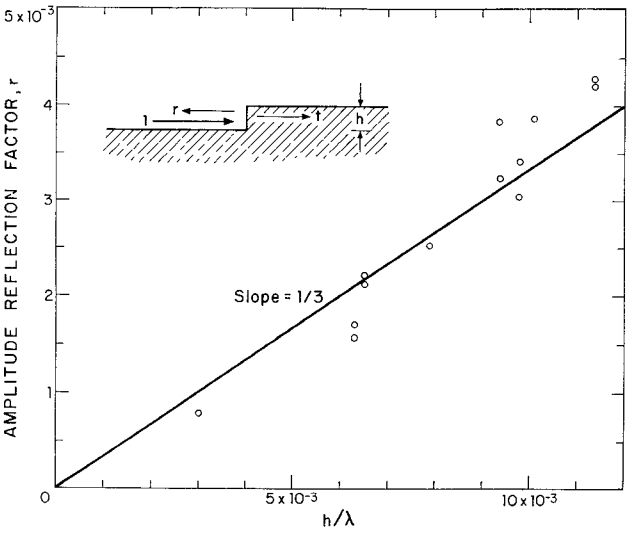

Fig. 3. Amplitude reflectivity of a step in Y–Z $LiNbO_3$ as a function of the normalized step height h/λ as deduced from measurements of a large array of grooves.

On the basis of a simple dimensional argument, as well as the explicit model of Li [13], r, the reflectivity of a step of height h in a $LiNbO_3$ surface, should be a function of h/λ (λ equals surface wavelength) and, for small values of h/λ, r should be linear in h/λ. Li's calculations imply that the proportionality constant is approximately $\frac{1}{3}$, a value consistent with the results shown in Fig. 3. The results presented in Fig. 3 also indicate that the reflectivity of portions of a grating can be adjusted by controlling the local groove depth. As will be discussed in detail later, this technique was used to achieve internal amplitude weighting in the RAC.

In Fig. 4 the frequency of maximum reflection of the normal-incidence gratings is plotted as a function of h/λ. These data indicate that the velocity of a surface wave traveling in a grating is less than the velocity of the wave on the free surface. Such velocity perturbations go rapidly to zero as h/λ is reduced. In the case of the prototype RAC ($h/\lambda \approx 6\times10^{-3}$), the effect was immeasurably small (less than 1 part in 10^4) and phase errors were negligible. On the other hand, for reflection-grating devices having small time–bandwidth products, and therefore a small number of effective reflectors at any frequency, the grooves would be much deeper and such

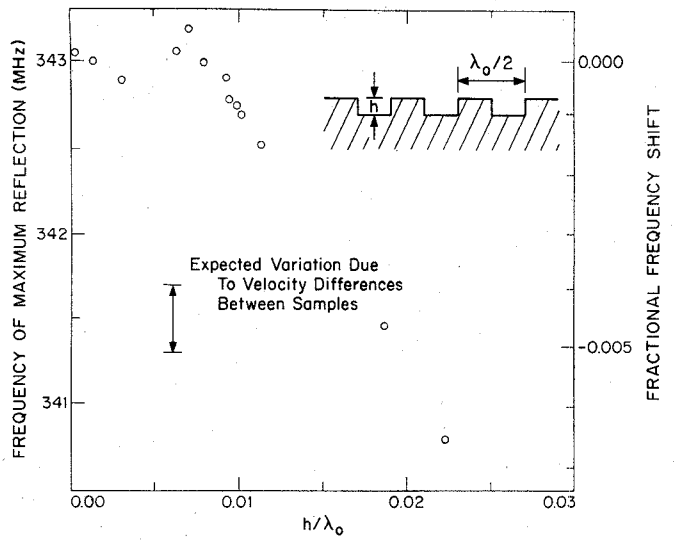

Fig. 4. Shift in frequency of maximum reflection for a periodic array of grooves as a function of groove depth h. The values of h/λ in the prototype RAC were on the order of 0.006.

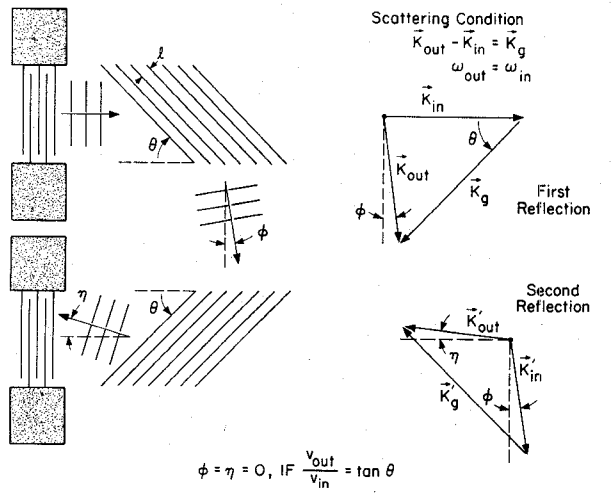

Fig. 5. Scattering-vector relations for reflection from symmetrically placed periodic gratings on an elastically anisotropic surface. The input and output transducers, wavefronts, and gratings of a RAC are also shown schematically.

velocity perturbations could be troublesome. Conversely, grating arrays with a large number of shallow grooves are more likely to be free of these second-order effects.

B. *Reflection at Oblique Incidence from Periodic Gratings*

The analysis of the reflection of surface waves on elastically anisotropic surfaces requires a generalization of the simple reflection laws. A grating with periodicity l may be characterized by a scattering vector $\boldsymbol{K}_g$, where $|\boldsymbol{K}_g| = 2\pi/l$, as shown in Fig. 5. The wave vectors $\boldsymbol{K}_{\text{in}}$ and $\boldsymbol{K}_{\text{out}}$ of the incident and outgoing waves at the first reflector must be related by $\boldsymbol{K}_{\text{out}} - \boldsymbol{K}_{\text{in}} = \boldsymbol{K}_g$. For a right-angle reflection to occur the condition $\tan\theta = v_{\text{out}}/v_{\text{in}}$ must be satisfied, where v_{out} and v_{in} are the phase velocities of the outgoing and incident waves. Thus the reflection of Z-directed waves into the X direction in a RAC requires that $\theta = \arctan v_x/v_z$. A series of experiments were performed in order to determine the proper value of θ.

In a test device, surface waves were reflected off a symmetrical pair of oblique incidence periodic gratings. The grating angle was established by calculations of v_x and v_z [14]–[16] based on the best available data on the elastic and piezoelectric parameters for $LiNbO_3$. Electrostatic probe measurements [17] of the reflected wavefronts showed that the surface waves were not reflected at 90 deg and that more accurate values of v_x and v_z would be required to establish the proper grating angle. These velocities were measured to high accuracy by means of an electrostatic probe [18]. The velocity of X-directed waves proved to be approximately 1.5 percent lower than the calculated value. Among 15 samples from 4 commercial sources, arctan (v_x/v_z) varied from 46.72 to 46.90 deg. Sixty percent of the samples lay in the range 46.82 ± 0.04 deg. This error bracket is the range of anisotropy that will yield less than 1-dB misalignment loss at the output transducer for an acoustic beam 100 wavelengths wide. With this in mind, 46.82 deg was chosen as the grating angle in the RAC device. Only one of the 12 pieces of $LiNbO_3$ used to produce RAC devices had an anisotropy outside the 1-dB limit.

If the symmetrically placed reflectors in a RAC device are set to the proper angle for 90 deg reflections, several effects act to suppress spurious bulk-wave signals at the output transducer. If either the incident or outgoing wave were a bulk wave, its velocity would be higher and its wave vector smaller than that of a surface wave. Thus the scattering condition would imply nonzero values of the angles ϕ and η defined in Fig. 5. Therefore, any spurious wave would either miss the output transducer or arrive there with a nonzero angle of incidence and thus be suppressed. A second effect further rejects spurious signals. The upper diagram in Fig. 5 shows the scattering relation for the first reflection, while the lower diagram illustrates the condition for the second reflection. If ϕ and η are nonzero, $|\boldsymbol{K}_{\text{out}}'|$ after two reflections is not equal to $|\boldsymbol{K}_{\text{in}}|$. In other words, a spurious wave which reflects off the first grating will be at the wrong frequency to reflect off the second grating. Because of these mode-filtering effects, RAC devices have proven to be quite free of spurious bulk-wave signals.

Direct measurements of the surface-wave reflection coefficients at oblique incidence were not made. However, our initial estimate that the value of r at the angle of incidence used in the RAC is approximately the same as the value of r at normal incidence proved adequate for the initial design. In order to avoid multiple reflections without excessive insertion loss, we aimed for a total reflection loss in the prototype RAC of 20 dB. An estimate of the number of effective grooves contributing to the reflection at any one frequency was used to calculate the desired reflectivity per groove edge and thereby the desired value of h/λ. At center frequency in the RAC, $h/\lambda \approx 6 \times 10^{-3}$ and $h \approx 1000$ Å. We have not made a thorough study of the phase and amplitude anomalies that arise as reflection loss is lowered, but it remains an open possibility that lower insertion loss could have been achieved without seriously degrading the performance of the prototype RAC.

C. *Transducer Design*

In the RAC configuration, the reflection grating performs the pulse compression. All that is required of the transducers is that they launch and receive surface waves with an adequate transduction loss, linear phase, and smoothly varying amplitude response over the band of interest. As will be seen below, smooth variations in amplitude response can be compensated by varying the etch depth within the grating.

In order to achieve simplicity in the initial RAC design, periodic interdigital transducers were chosen. Given the limitations of such transducers, we chose to operate over a fractional bandwidth of only 25 percent. Thus a center fre-

quency of 200 MHz was chosen to yield the 50-MHz operating bandwidth.

The choice of the acoustic beamwidth was influenced by several factors. As the beam is widened, diffraction losses are reduced, the radiation resistance of the transducers decreases toward the optimum value of 50 Ω, and spurious bulk waves are more strongly rejected. On the other hand, a narrow beam results in less electrode conduction loss, and loss due to slight surface wavefront misorientations is reduced. As a compromise, a beamwidth of 100 acoustic wavelengths was chosen.

The transducers were tested in a simple delay-line configuration. When inserted directly in a 50-Ω system, an insertion loss of 33 dB was obtained. With a matching circuit consisting of a lumped transformer and inductors, the insertion loss was 17 dB. With matching, the phase response remained highly linear with a phase deviation from linearity less than ±2.0 deg over a 50-MHz bandwidth.

III. Large Time–Bandwidth Design Considerations

A. Transfer-Function Analysis

A first-order analysis of the transfer function of a symmetric reflecting array may be made using a model which is very similar to the δ-function model of an interdigital array [4]. In this model, a δ-function reflection of strength r_m is placed on the mth edge in the array of reflecting grooves. If multiple reflections are ignored and the incident acoustic wave is assumed to be negligibly attenuated as it passes through the reflecting array, the overall transfer function for a symmetrical set of reflectors is[1]

$$H_0(\omega) = \sum_{m,n=1}^{2N} r_m r_n \gamma_{mn} e^{-j(\omega/v_z)(x_m+x_n)} \tag{1}$$

where N is the number of grooves in each of the two rows of the reflective array, and x_m is the distance from the first edge to the mth edge in a row as measured along the center line of the incident acoustic beam. All constant delays have been ignored in (1). The reflection overlap factor γ_{mn} measures the fraction of the nth edge in the second row illuminated by the mth edge in the first row of reflectors:

$$\gamma_{mn} = 1 - \frac{|x_m - x_n|}{d'}, \qquad \text{if } |x_m - x_n| < d'$$

$$\gamma_{mn} = 0, \qquad \text{if } |x_m - x_n| > d' \tag{2}$$

where d' is the projection of a reflecting edge along the X direction. For an isotropic substrate, d' is equal to the incident beamwidth d. The γ_{mn} factor renders the double sum in (1) unseparable. It should be noted that the twice-reflected acoustic beam has a nonuniform amplitude profile, and the factor γ_{mn} properly accounts for the effective wave amplitude as detected by the output transducer.[2]

If we assume that the reflection coefficient at each edge is a real quantity, as is assumed in the model of Sittig and Coquin [8], then the phase inversion between reflections at the front and back edges of a groove is summarized by $r_1 = -r_2$, $r_3 = -r_4$, etc. Drawing on the results of the normal-incidence reflection measurements,

$$|r_m| = C\frac{h_m}{\lambda}, \text{ to} \qquad C \approx 1/3.$$

If we now enumerate the grooves in each half of the grating by indices p and q, and let x_p be the position of the center of the pth groove, (1) can be rewritten:

$$H_0(\omega) = \sum_{p,q=1}^{N} (C\omega/\pi v_z)^2 h_p h_q \sin(\omega W_p/2v_z) \cdot \sin(\omega W_q/2v_z)\gamma_{pq} e^{-j(\omega/v_z)(x_p+x_q)} \tag{3}$$

where W_p is the width of the pth groove as measured along the Z direction, and h_p is the depth of the pth groove. In writing (3), we have assumed that $W_p \ll d'$.

From (3) it can be seen that internal weighting of the pattern can be achieved by varying the depth h_p. If the groove width is held constant, as in the prototype RAC design, (3) becomes:

$$H_0(\omega) = (C\omega/\pi v_z)^2 \sin^2(\omega W/2v_z) \sum_{p,q=1}^{N} h_p h_q \gamma_{pq} \cdot e^{-j(\omega/v_z)(x_p+x_q)}. \tag{4}$$

The factor in front of the summation imposes a slow amplitude variation on the response which tends to peak at a frequency slightly above

$$\omega = \pi v_z/W \qquad \text{or } W = \lambda/2. \tag{5}$$

The overall response of an ideal reflective-array device will be the product of $H_0(\omega)$ and the transfer function of the transducers. For a real device, losses due to beam steering, attenuation, and diffraction must be included.

If we now consider the case of a matched filter for a linear FM signal, the center positions of the grooves are given by:

$$x_p - x_1 = \left(\frac{v_z f_1 \Delta T}{2\Delta f}\right)[1 - (1 - (4\Delta f/f_1^2 \Delta T)(p-1))^{1/2}], \qquad p = 1, 2, \cdots, f_0\Delta T/2 + 1 \tag{6}$$

where ΔT is the pulse duration, Δf is the FM bandwidth, f_0 is the center frequency, $f_1 = f_0 + \Delta f/2$ is the highest frequency in the FM pulse.[3]

The initial goal for the prototype RAC was a bandwidth of 50 MHz and pulse length of 30 μs. However, we designed a grating pattern with the same FM slope but twice the minimum time and twice the bandwidth. Thus each half of the grating pattern was 30 μs or 10.4 cm long for a total dispersion of 60 μs, and a bandwidth of 100 MHz. This excess grating bandwidth allowed us to weight the device outside the band of interest and thus suppress band-edge ripples. In addition, the excess grating opened the possibility that devices with time–bandwidth products well above 1500 might be achieved through the use of wider bandwidth transducers.

[1] In this analysis we have generally tried to use the same nomenclature and symbols as [9].

[2] In principle, it would be possible to weight the time-domain response of a RAC by varying the length of the reflectors in a grating ("apodizing") in order to vary the magnitude of γ_{mn}. However, we chose not to do this because each change in weighting would then require a change in grating geometry. Also we wanted to avoid diffraction loss and possible wavefront distortion.

[3] The evaluation of $H_0(\omega)$ is difficult for a large array of reflectors because of the large number of terms in the double sum. Exact evaluation has not been carried out for the prototype RAC. However, efficient computational procedures which judiciously invoke the symmetry of the RAC configuration have been developed [19].

B. Velocity Errors

If v_z varies from the value assumed (1)–(6), the pulse compressor will no longer be the matched filter for the specified linear FM signal. The quadratic phase distortion arising from a change in v_z will cause a broadening and decrease in amplitude of the compressed pulse as well as an increase in the level of time sidelobes [21]. In addition, a change in v_z will cause a change in the delay between the input signal and the peak of the compressed pulse or, equivalently, a range error. The degree to which v_z must match the desired value depends on the type and magnitude of the errors which can be tolerated. Control of velocity variations becomes more critical as the time–bandwidth product of a device increases.

A change in v_z can arise from any one of four sources: grating perturbations, crystal misorientation, material variation [18], and temperature. As discussed previously, velocity perturbations in the grating can be avoided by limiting the value of h/λ. For $LiNbO_3$, the value of v_z will shift by 620 ppm for every degree that the crystalline Z axis is rotated out of the surface plane [16]. Y–Z $LiNbO_3$ has a temperature coefficient of delay equal to 90 ppm per °C.[4] As discussed below, the prototype RAC had to be thermostatted, and in such cases, the set temperature can be adjusted so as to compensate for the velocity shifts caused by other effects. For example, a 20-°C range of thermostatting temperature can compensate for material variations corresponding to a ± 2-m/s variation in v_z, and a crystalline misorientation of ± 0.5 deg of rotation.

Once the thermostatting temperature is set, the required degree of stability can be estimated on the basis of the temperature coefficient of delay. For example, in the prototype RAC device with a time–bandwidth product of 1500, a 1°C change in temperature causes a quadratic phase error at the edges of the band equal to 12.1 deg of phase. Such an error has a barely noticeable effect on the shape of the pulse for the case of a pulse compressor with no weighting [21]. However, a device which is heavily weighted for sidelobe suppression is much more tolerant of phase errors. For example, in the prototype RAC, a temperature variation of 7.4°C causes a 90-deg phase error at the band edges, but with weighting, the sidelobes remain below 38 dB and pulsewidth is essentially unaffected [21]. The allowed temperature deviation decreases inversely as the time–bandwidth product of a device and system limitations on the achievable temperature control may preclude the use of $LiNnO_3$ in some large time–bandwidth devices. In such instances a substrate material with a low temperature coefficient of delay, such as S–T-cut quartz, would be required.

The range error in a pulse compressor is a function of the FM slope, center frequency, and fixed delays. For the prototype RAC, a 1-°C shift in temperature causes a range error of 7.8 ns, which is approximately $\frac{1}{3}$ of the compressed pulsewidth. In most applications such an error is negligible as long as the rate of temperature change is sufficiently slow.

In the RAC configuration, temperature induced changes in the anisotropy can cause misalignment loss. However, our measurements of the coefficients of delay for X- and Z-directed waves on $LiNbO_3$ show that the X coefficient is only 14 ppm less than the Z coefficient. Thus a 100-°C shift in temperature would cause only a 1-dB misalignment loss. While such an effect is negligible for $LiNbO_3$, it may pose a problem in other materials whose temperature coefficients along perpendicular directions differ by a large amount.

[4] This value was measured in our laboratory. Reference [20] gives 85 ppm per °C. Reference [16] calculates a value of 94 ppm per °C.

IV. Fabrication

A. Crystal Orientation

Because of the large anisotropy of $LiNbO_3$, a substrate must be carefully oriented relative to the crystalline axes. Each of the three possible orientational errors gives rise to a different type of device degradation. Let us define α, β, and γ as the angles of rotation of the face normals of a rectangular substrate of $LiNbO_3$ about the X, Y, and Z crystalline axes, respectively. For perfect Y-cut, with X and Z axes perpendicular to their respective faces, $\alpha=\beta=\gamma=0$.

As mentioned above, v_z changes linearly with α at a rate of 620 ppm per deg. In addition, v_x changes linearly in the opposite sense to v_z at a rate of 1013-ppm-per-deg change in α [16]. As a result, the twice-reflected wavefront in a RAC changes direction by 0.19 deg for a 1-deg change in α. [Recall that the desired grating angle is equal to arctan (v_x/v_z).] In order to keep the loss caused by wavefront misalignment below 1 dB in a device with a 100-λ-wide beam, $|\alpha|$ must be less than 0.8 deg.

Nonzero values of β and γ cause only second-order changes in v_z, but do cause beam steering with resultant loss over long propagation paths. A loss of 1 dB would occur at the low-frequency (150 MHz) end of the prototype RAC for $\beta=0.06$ deg or $\gamma=0.4$ deg.

From the foregoing discussion, it is clear that substrate orientation must be carefully controlled. Our specifications to commercial suppliers were $|\alpha|<0.1$ deg, $|\beta|<0.1$ deg, and $|\gamma|<0.5$ deg. However, these specifications were seldom achieved, and we were forced to independently check crystalline orientation before device fabrication. A technique was developed which allowed the value of β to be measured to ± 0.05 deg on a polarizing microscope. With this measurement the RAC patterns could be subsequently aligned with the Z crystalline axis. The values of α and γ were measured to ± 0.02 deg on an X-ray diffractometer. The first 3 RAC devices were on substrates with $|\gamma|>2$ deg and correspondingly large loss occurred at the low-frequency end of the band.

B. Photolithography

Three separate photolithographic steps were required in the fabrication of the prototype RAC. In the first, the input and output transducers were produced by means of a lift-off technique [22]. The metal film was 300 Å of chromium and 1300 Å of gold. In the second step, the $LiNbO_3$ substrate was recoated with photoresist, and the grating pattern exposed and developed. The areas left unprotected by photoresist were then sputter etched in an argon ion beam. After sputter etching and the initial testing to determine wavefront alignment, the third photolithographic step placed wavefront correcting prisms (if needed) and feedthrough shields around the 2 transducers. Separate photomasks were used in each of the 3 steps. Each photomask included special clear areas and alignment marks which permitted the axes of the transducers, the grating, and the prisms to be aligned parallel to each other and parallel to the measured crystalline Z axis to within 0.01 deg, well within the required tolerance. The photomask patterns were in 800-Å-thick chromium on Corning-type 0211 glass, 1/5 mm thick. The use of such flexible photomasks has been described elsewhere [22]. The photo-

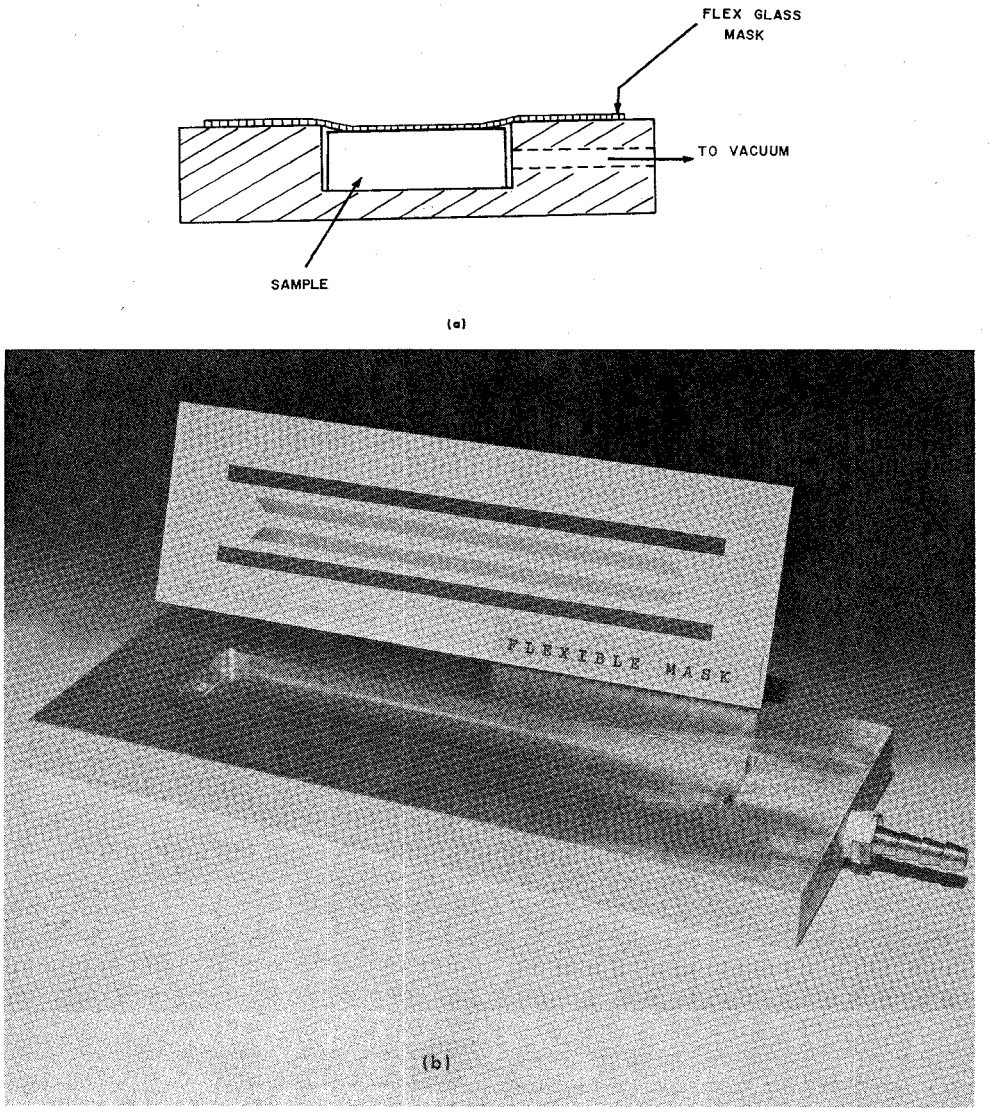

Fig. 6. (a) Schematic diagram of vacuum frame for use with a flexible glass photomask. (b) RAC photomask and vacuum frame.

masks were replicas made by contact printing from master plates obtained from commercial sources.

The fabrication of the grating pattern demanded special techniques because of the large number of stripes (12 000), the large area occupied (3.6 cm^2), and the stripe-positioning precision required. Each stripe of the grating pattern was separately exposed in a photographic emulsion plate. The placement of each stripe was controlled by a laser-interferometer system having a least count of 800 Å. Positioning errors in the grating mask translate into phase errors in the final RAC device. For example, a stripe-placement error of 1000 Å corresponds to 2 deg of phase error. However, because at any given frequency there were about 80 cooperating reflectors, a small percentage of stripes could be displaced from their desired positions, as long as such placement errors were random [9]. We were not able to check the precision of the grating patterns independent of testing RAC device performance.

In order to simplify the task of producing the grating master plate, it was specified that the stripe width as measured in the Z direction be constant throughout the array at $\lambda_0/2$, where λ_0 is the wavelength at 200 MHz.[5] However, in the pattern used to make the prototype RAC, the grooves were somewhat wider than this, and correspondingly the peak response shifted to a lower frequency than intended [see (4)].

The $LiNbO_3$ substrates and the thin 0211 glass plates on which the grating photomasks were made were too large to be coated with photoresist by the usual spin-coating method Instead, dip coating was used which resulted in films about 5000 Å thick and uniform to within about ± 100 Å.

Because the surface-wave reflection process is a localized mechanical effect, defects in the reflection grating, such as broken or joined stripes, can be tolerated provided that in the area occupied by any group of cooperating reflectors the

[5] It is noteworthy that the width of the grooves as measured perpendicular to their edges is $\sqrt{2}$ times wider than the width of the electrodes in an interdigital transducer operating at the same frequency. Thus, for the same photomask resolution, a higher operating frequency can be achieved with RAC.

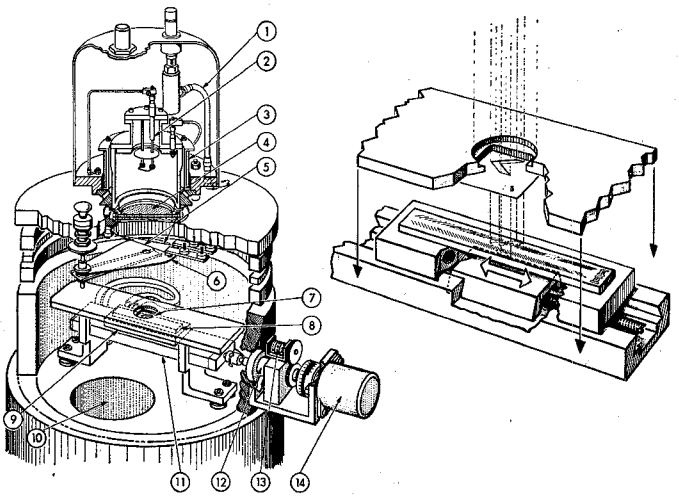

Fig. 7. Ion-beam etching apparatus: ① argon gas inlet, ② arc filament, ③ magnet, ④ ion-beam extraction grids, ⑤ neutralizing filament, ⑥ shutter, ⑦ chevron aperture, ⑧ RAC substrate, ⑨ water-cooled sample platform, ⑩ pumping port, ⑪ micrometer-slide assembly, ⑫ rotary-motion high-vacuum feedthrough, ⑬ position indicator, ⑭ stepping motor.

fractional area of defects is small. Such defects were present in the original master plate and additional ones were introduced in the processes of making the replica photomask and transferring the pattern onto the $LiNbO_3$ substrate. In no case did we detect any anomalies in the electrical response which we could attribute to these grating defects.

The flexible glass photomask in conjunction with the simple vacuum frame shown in Fig. 6 enabled us to replicate the large area RAC grating in precisely the same way on each substrate. When the frame is evacuated, the flexible glass deforms to the contours of the substrate, thereby ensuring intimate contact with the photoresist film over the entire grating area. We found that this system is capable of replicating submicron details of the photomask. An occasional dust particle results in only a very localized defect. The intimacy of the contact prevents stripe widening due to diffraction and ensures that the photoresist profile has a sharp vertical character [22]. The latter is subsequently reproduced in the etched grooves.

C. Sputter Etching

Following exposure and development of the grating pattern, the substrate was mounted on the water-cooled sample platform of the ion-beam etching apparatus shown schematically in Fig. 7. The mechanical motion and associated control system were developed in our laboratory; the ion gun was obtained commercially.[6] The beam is neutralized after emerging from the gun by injecting electrons from a hot tungsten filament, thus enabling insulators to be etched.

We normally operated the ion-beam system at an energy of 500 eV and a current density of 0.8 mA/cm^2. This corresponds to an etching rate of 4.6 Å/s for $LiNbO_3$ and 2.5 Å/s for AZ1350H photoresist. As shown in Fig. 7, a chevron shaped aperture was placed in the beam between the gun and the substrate. The depth of etching at a given point depends on the total time that point is exposed to the beam, which could be varied by varying the rate at which the substrate was moved past the aperture. The chevron aperture had a width in the direction of travel of 5 mm, and was made from 0.1-mm-thick titanium foil. The sample platform was driven on a screw by a programmable stepping motor.

In order to sputter etch a device so as to achieve a desired amplitude response, it was assumed that the amplitude of the overall transfer function at any given frequency is proportional to the square of the depth of the grooves resonant at that frequency [see (4)]. Thus, from the measured response of a device etched to a constant depth throughout the grating, the depth as a function of grating position which would be required in order to obtain a desired response was calculated. Computer generated instructions to the stepping motor varied the substrate drive speed past the chevron aperture in such a manner as to achieve the depth function.

During the course of a run ($\sim$1 h), we stabilized the etching rate by using a regulated accelerating voltage and manually maintaining the ion current density constant to within about ± 2 percent. This was necessary because a 6-percent variation in etched depth corresponds to a 1-dB variation in insertion loss. Depth measurements were made on a number of gratings by Tolansky interferometry. On the basis of these measurements and our weighting experiments, we believe the etching rate was constant during any given run to within ± 3 percent.

The Tolansky interferograms as well as scanning electron micrographs indicated that the etched grooves had well-defined vertical sides, and that the smoothness of the groove bottoms was comparable to that of the original substrate surface.

One disadvantage of ion-beam etching is that a very thin quasi-continuous metallic film is left on the substrate. We attribute this to the forward sputtering of the titanium aperture. (Titanium was chosen because of its relatively low sputtering yield.) However, the tungsten neutralizing filament and the molybdenum accelerating electrodes also forward sputter to some degree, the rate being highly dependent on system parameters. The metallic film was highly attenuating to surface waves [23] and had to be removed by chemical etching.

D. Wavefront Correction, Isolation, and Packaging

After fabrication of the reflection grating, the RAC device was temporarily mounted in a jig which provided electrical contact to the transducers by spring loaded posts. The wavefront orientation was then checked by means of the electrostatic probe [17]. Following this initial test, a closed border of thin-film aluminum was placed around each transducer. When grounded, these isolation shields acted to short out the electric fields in the $LiNbO_3$ and strongly reduced direct leakage of signal between the input and output transducers. The substrate with its isolation shields was mounted in a package with a metal septum between transducers. A strip of indium under the septum firmly grounded the isolation shields to the package. With no matching circuitry, 90 dB of isolation was achieved, which is 36 dB below the typical value of peak CW acoustic signal. This degree of isolation is adequate for most systems applications since the feedthrough is gated out during pulse expansion and is reduced further on

[6] The ion gun was manufactured by Thomson-CSF, Corbeville, France, and marketed in the United States by Veeco Instruments, Inc.

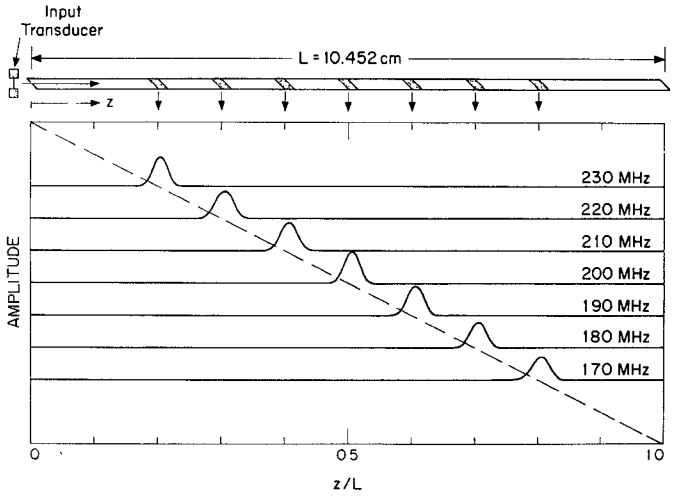

Fig. 8. Amplitude of surface waves reflected into the X direction on the prototype RAC as a function of position in the Z direction. As the frequency changes, the point of maximum reflection moves linearly down the array. The shaded portions of the RAC grating (top of figure) indicate the regions which are calculated to produce the dominant reflection at each frequency.

compression by the compression gain (32 dB for the prototype RAC).

V. Device Performance

It is fundamental to the operation of a RAC that signals of different frequency are strongly reflected at different positions in the grating. To check this, the amplitudes of X-directed waves in the gap between the grating halves were measured as a function of position in the Z direction at several fixed frequencies. To within the accuracy of the measurement (± 0.5 mm), the z position corresponding to maximum reflected signal increased linearly with decreasing frequency, as shown in Fig. 8.

To date, 12 RAC devices have been made. The first 3 were fabricated on poorly oriented substrates ($\gamma > 2$ deg) and beam-profile measurements with the electrostatic probe indicated that beam steering was large ($\simeq 0.25$ deg). These devices exhibited correspondingly high loss at low frequencies. The first 2 were etched to uniform depth, and on the basis of their amplitude response, a control tape was generated for variable depth etching of the third device (our no. 111) which was intended to have a flat amplitude response. Fortunately, the third device's substrate had approximately the same misorientation as the first 2, so that the weighting procedure produced a nearly flat amplitude response.

Several RAC devices have been constructed with uniform etch depth on well-oriented substrates, and each had an unmatched insertion loss in the range 53–55 dB. This degree of reproducibility reflects the reproducibility of the ion-beam etching, where a 6-percent change in etch depth would yield a 1-dB change in insertion loss. The minimum insertion loss of the transducers alone was 33 dB, so that the sum of reflection, propagation, and diffraction losses was about 21 dB, a value close to the original goal of 20 dB. Calculations of the diffraction loss [24] indicate a maximum value of 1.4 dB at the lowest frequency. This is entirely consistent with the well-defined beam profiles measured at various distances from the transducers. Insertion loss measurements with matched transducers indicated that the transduction loss could be reduced by 16 dB, resulting in a total device insertion loss of

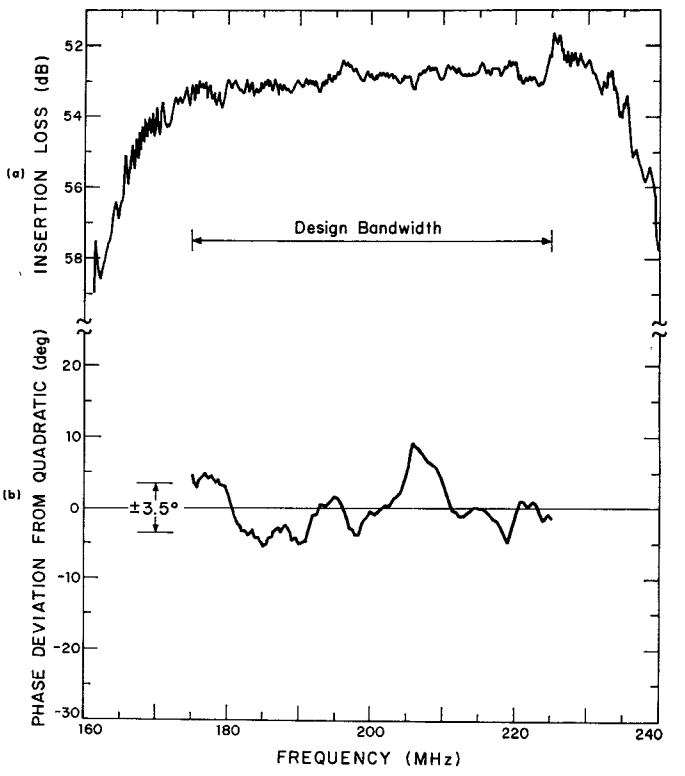

Fig. 9. (a) Insertion loss versus frequency for device no. 111, a reflective-array compressor weighted for flat amplitude response over a 50-MHz bandwidth. The device had no external matching or weighting. (b) Phase response. The data are deviations of the measured phase from a quadratic fit versus frequency. The rms deviation is 3.5 deg. Total phase change over the indicated band is 5.4×10^5 deg. The phase anomaly near 208 MHz was found in other devices, and appears to be inherent in the photomask of the grating pattern.

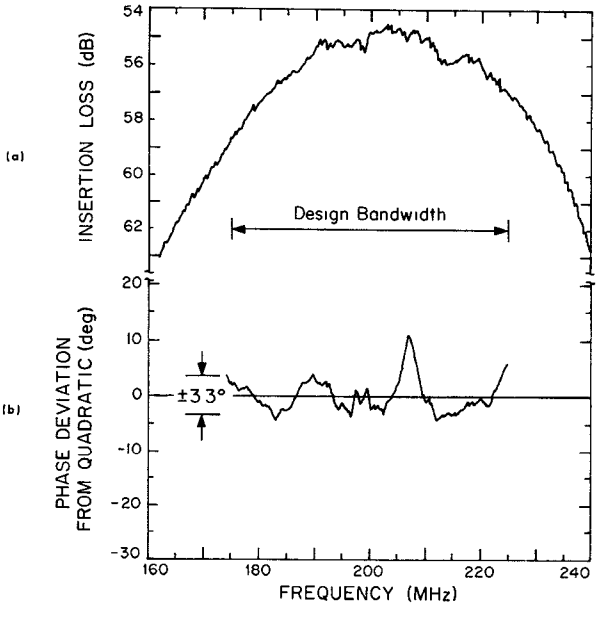

Fig. 10. (a) Insertion loss versus frequency for device no. 116, a reflective-array compressor etched to uniform depth. The device had no external matching or weighting. (b) Phase response plotted as in Fig. 9. The rms deviation from a quadratic fit is 3.3 deg.

38 dB. However, we have not produced a RAC with matched transducers because the unmatched transducers provided adequate dynamic range on compression. In addition, we have focused our attention on the performance of the grating

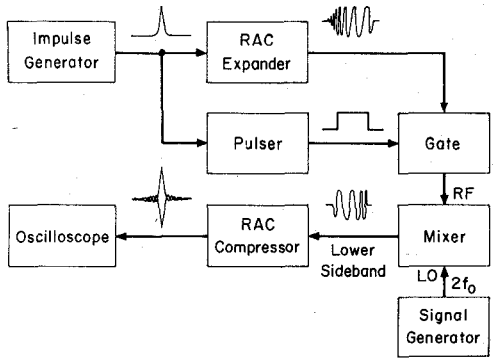

Fig. 11. Block diagram of the circuitry used for tests of the pulse compression performance of the prototype RAC.

and did not wish to introduce the matching as an additional variable.

The amplitude and phase responses of several RAC devices were measured on a computerized network analyzer. This instrument completed the measurement of each device in about 30 min, a period during which the temperature of the thermostatted RAC drifted slowly by at most 4×10^{-3}°C. Thus temperature induced phase errors were negligible. Direct leakage resulted in a fast ripple on the phase response of 1–2 electrical degrees. This ripple was subtracted out before plotting the phase response in Figs. 9 and 10. Fig. 9 shows the characteristics of device no. 111, which was etched so as to achieve a flat amplitude response from 170 to 230 MHz and cosinusoidal tails over the remainder of the 100 MHz of grating bandwidth. Fig. 10 displays the characteristics of device no. 116, which was etched to uniform depth on a well-oriented substrate.

For an ideal linear FM signal, the phase is a quadratic function of frequency. Accordingly, the phase response of each device was fitted by a quadratic and the deviations from the best fit for 2 devices are plotted in Figs. 9 and 10. The rms deviations of the phase were approximately 3.5 deg over a 50-MHz bandwidth for all devices measured. However, the quadratic coefficients, or equivalently the FM slopes, were slightly different for each device. The quality of phase response that has been achieved implies that, with appropriate weighting, time sidelobes below 35 dB can be obtained with these pulse compressors.

In a pulse compression test, device no. 111 was used as the pulse expander and device no. 116 as the pulse compressor. The FM slopes of the 2 devices were matched by thermostating device no. 111 about 5°C above the temperature of device no. 116. Because of the high expansion loss (~85 dB), a large amplitude impulse was required to bring the expanded pulse above noise. This impulse was derived from a charged-line pulser. After spectral inversion and gating, the pulse was recompressed in device no. 116 (see Fig. 11).

The compression results obtained when the expanded pulse was gated over a 30-μs interval are shown in Figs. 12 and 13. The 4-dB width of the compressed pulse is approximately 20 ns, the value expected for a 50-MHz bandwidth. The compression ratio of 1500 is clearly demonstrated. As shown in Fig. 13, the near-in sidelobes are 15 dB below the peak of the compressed pulse. This is about 2 dB less than the 13-dB sidelobes which would be expected for a device with flat amplitude response, the additional depression resulting from the slight rounding of the passband in device

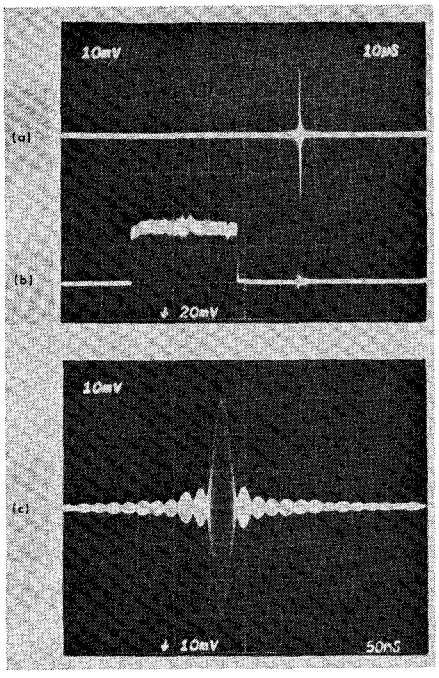

Fig. 12. Pulse compression test in which a 30-μs 50-MHz bandwidth linear FM pulse was obtained by impulsing device no. 111. The expanded pulse was recompressed in device no. 116. (a) Compressed pulse. Horizontal scale is 10 μs/div. (b) Detected envelope of the expanded pulse. (c) Expanded display of compressed pulse. Horizontal scale is 50 ns/div. The 4-dB width of the compressed pulse is 20 ns.

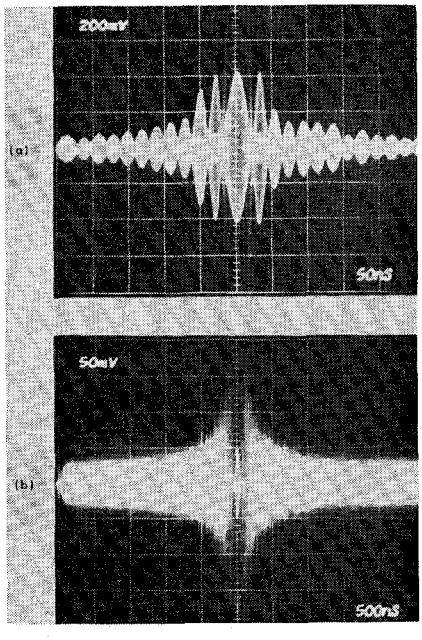

Fig. 13. (a) Double exposure of compressed pulse shown in Fig. 12 with 15-dB difference in attenuation between exposures. Horizontal scale is 50 ns/div. (b) Double exposure of the same compressed pulse with 40-dB difference in attenuation between exposures. The 40-dB level is 2 divisions peak to peak. Sidelobes fall off regularly. Far-out spurious sidelobes are well below 40 dB. Horizontal scale is 500 ns/div.

no. 116. The approximately sin x/x compressed pulse pattern falls off in a regular way, and far-out spurious sidelobes are well below 40 dB.

These same 2 devices were also tested with no gating of the expanded pulse, Figs. 14 and 15. In this case, both devices operated over a range of frequencies in which the phase and amplitude responses were much poorer than in the

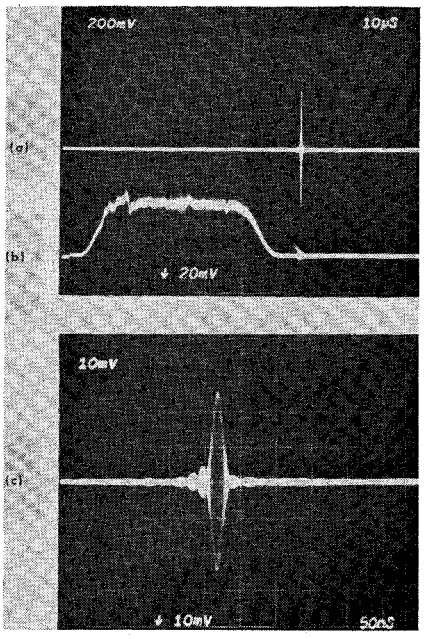

Fig. 14. Pulse compression test in which the expanded pulse from device no. 111 is not gated. (a) Compressed pulse. Horizontal scale is 10 μs/div. (b) Detected envelope of the expanded pulse. (c) Compressed pulse. Horizontal scale is 50 ns/div. The half-power width of the compressed pulse is 12 ns.

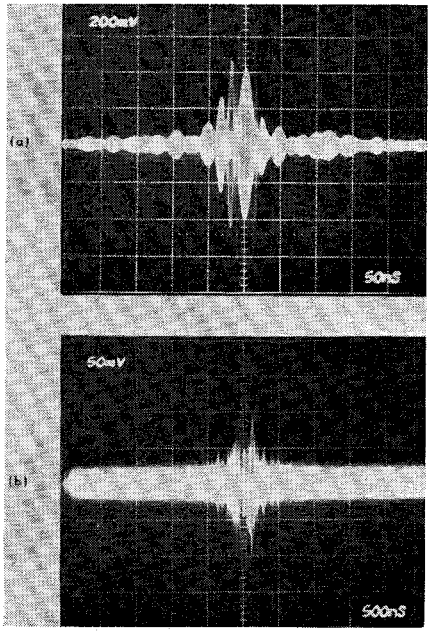

Fig. 15. (a) Double exposure of compressed pulse shown in Fig. 14 with 16-dB difference in attenuation between exposures. Horizontal scale is 50 ns/div. (b) Double exposure of compressed pulse with 40-dB difference in attenuation between exposures. The 40-dB level is 2 divisions peak to peak. Horizontal scale is 500 ns/div.

50-MHz design bandwidth. In the expanded pulse, there is no evidence of spurious signals occurring before or after the main surface-wave signal. The compressed pulse has a half-width of only 12 ns (Fig. 14), thus achieving a compression ratio of about 4000. As expected, the sidelobe pattern is less than ideal, although there is no evidence of far-out spurious sidelobes.

The above results were achieved with 5-electrode transducers. The bandwidth of these transducers was the major restriction on the time–bandwidth product achievable with this RAC design. The grating itself appeared to operate well over the full 100-MHz bandwidth. In order to access more of this bandwidth, a RAC with 3-electrode transducers was fabricated. A time–bandwidth product of more than 3000 was obtained with a modest sacrifice in phase fidelity. This degradation in phase response was largely traceable to phase ripples in the transducer response. Measurement with an electrostatic probe placed in front of the input transducer indicated that relatively high-level spurious bulk modes were being generated. However, such spurious signals were undedetectable at the output transducer, illustrating the efficient mode-filtering action of the RAC configuration.

VI. Summary

We have demonstrated a new surface-wave device concept based on the controlled reflection of surface waves from arrays of step discontinuities. The technology of producing and evaluating reflection gratings has been explored. It has been shown that the reflection process is sufficiently simple that a complex device can be designed using a first-order theory.

For small time–bandwidth devices, the RAC configuration has higher insertion loss and requires more involved processing than interdigital devices. However, for devices with low spurious levels or large capacities, the RAC configuration has a number of intrinsic and practical advantages. The mode-filtering action of the oblique grating leads to low spurious levels. The problems of unwanted reflections, velocity shifts, reradiation, propagation loss, and dispersion inherent in interdigital-electrode transducers are avoided. For a given substrate, RAC provides twice the dispersion of an in-line device because of the folded path. Photolithographic and mask-fabrication problems are reduced and wider bandwidths appear achievable because defects can be tolerated. Since amplitude weighting is achieved in the sputter etching, changes in weighting do not demand a new mask design. Transducer design is largely separated from considerations of the filtering function thereby permitting optimum designs of transducers and gratings.

On the basis of our experience with the prototype RAC we can make an estimate of the ultimate capacities achievable with the RAC configuration. We believe that the principle of grating reflectors has no fundamental frequency limitations. However, problems of photomask generation impose practical constraints. State of the art in interferometer-controlled pattern generators yields an accuracy in the placement of reflecting grooves which restricts the bandwidth to about 500 MHz. Optical projection schemes are limited in minimum linewidth to about 1 μm which implies a similar bandwidth limitation. On $LiNbO_3$, the dynamic range will be seriously decreased because of propagation losses for devices with 500-MHz bandwidth and dispersions of more than 10 μs. Maximum dispersion at bandwidths below about 50 MHz will be limited by the size of available substrates. Dispersions of 90 μs on $LiNbO_3$ and 200 μs on quartz or bismuth germanium oxide appear achievable. Beam steering, diffraction, and temperature sensitivity probably impose a limitation of about 10^4 on the time–bandwidth product. These combinations of

bandwidth and dispersion time lie far beyond what is currently achievable by any other means and for this reason, we feel that the RAC configuration shows promise of significantly extending the capacities of pulse compressors.

Acknowledgment

The authors wish to thank E. Stern for his original insights which stimulated the development of the RAC and for his tireless encouragement throughout this work. W. T. Brogan and N. Efremow did the ion-beam etching and photolithography. J. A. Alusow and S. S. Cupoli provided capable assistance in device testing and evaluation. The authors also wish to thank R. C. M. Li for many helpful discussions.

References

[1] R. M. White, "Surface elastic waves," *Proc. IEEE*, vol. 58, pp. 1238–1276, Aug. 1970.
[2] G. S. Kino and H. Matthews, "Signal processing in acoustic surface-wave devices," *IEEE Spectrum*, vol 8, pp. 22–35, Aug. 1971.
[3] J. Vollmer and D. Gandolfo, "Microsonics," *Science*, vol. 175, pp. 129–133, Jan. 1972.
[4] R. H. Tancrell and M. G. Holland, "Acoustic surface wave filters," *Proc. IEEE*, vol. 59, pp. 393–409, Mar. 1971.
[5] W. R. Smith, H. M. Gerard, and W. R. Jones, "Analysis and design of dispersive interdigital surface-wave transducers," *IEEE Trans. Microwave Theory Tech.*, vol. MTT-20, pp. 458–471, July 1972.
[6] R. H. Tancrell and R. C. Williamson, "Wavefront distortion of acoustic surface waves from apodized interdigital transducers," *Appl. Phys. Lett.*, vol. 19, pp. 456–459, Dec. 1971.
[7] W. S. Jones, C. S. Hartmann, and T. D. Sturdivant, "Second order effects in surface wave devices," *IEEE Trans. Sonics Ultrason.*, vol. SU-19, pp. 368–377, July 1972.
[8] E. K. Sittig and G. A. Coquin, "Filters and dispersive delay lines using repetitively mismatched ultrasonic transmission lines," *IEEE Trans. Sonics Ultrason.*, vol. SU-15, pp. 111–119, Apr. 1968.
[9] T. A. Martin, "The IMCON pulse compression filter and its applications," *IEEE Trans. Microwave Theory Tech.*, this issue, pp. 186–194.
[10] J. Melngailis, J. M. Smith, and J. H. Cafarella, "Bandpass surface wave filters," in *Proc. 1972 IEEE Ultrasonics Symp.*, pp. 221–225, Oct. 1972.
[11] R. C. Williamson and H. I. Smith, "Large-time-bandwidth-product surface-wave pulse compressor employing reflective gratings," *Electron. Lett.*, vol. 8, pp. 401–402, Aug. 1972.
[12] ——, "The reflection of elastic surface waves from periodic arrays on *YZ* $LiNbO_3$," presented at the IEEE Ultrasonics Symp., Miami, Fla., Dec. 1971, Paper J-5.
[13] R. C. M. Li, "Analysis of surface wave reflection from a periodic array of grooves," in *Proc. 1972 IEEE Ultrasonics Symp.*, pp. 263–266, Oct. 1972.
[14] J. J. Campbell and W. R. Jones, "A method for estimating optimal crystal cuts and propagation directions for excitation of piezoelectric surface waves," *IEEE Trans. Sonics Ultrason.*, vol. SU-15, pp. 209–217, Oct. 1968.
[15] A. J. Slobodnik and E. D. Conway, "Microwave acoustics handbook," Air Force Cambridge Research Laboratory, Bedford, Mass., AFCRL-70-0164, Mar. 1970 (unpublished).
[16] A. J. Slobodnik, "The temperature coefficients of acoustic surface wave velocity and delay on lithium niobate, lithium tantalate, quartz and tellurium dioxide," Air Force Cambridge Research Laboratory, Bedford, Mass., AFCRL-72-0082, Dec. 1971 (unpublished).
[17] R. C. Williamson, "Improved electrostatic probe for measurement of elastic surface waves," *IEEE Trans. Sonics Ultrason.*, vol. SU-19, pp. 436–441, Oct. 1972.
[18] R. C. Williamson, "Measurement of the propagation characteristics of surface and bulk waves in $LiNbO_3$," in *Proc. 1972 IEEE Ultrasonics Symp.*, pp. 323–327, Oct. 1972.
[19] D. P. Olsen, "A frequency and time domain analysis of the IMCON II pulse compression delay line," Technology Service Corporation, Santa Monica, Calif., TSC-PD-080-64, July 1972 (unpublished).
[20] J. D. Maines, E. G. S. Paige, A. F. Saunders, and A. S. Young, "Simple technique for the accurate determination of delay-time variations in acoustic-surface-wave structures," *Electron. Lett.*, vol. 5, pp. 678–680, Dec. 1969.
[21] J. R. Klauder, A. C. Price, S. Darlington, and W. J. Albersheim, "The theory and design of chirp radars," *Bell Syst. Tech. J.*, vol. 39, pp. 745–808, July 1960.
[22] H. I. Smith, F. J. Bachner, and N. Efremow, "A high-yield photolithographic technique for surface wave devices," *J. Electrochem. Soc.*, vol. 118, pp. 821–825, May 1971.
[23] M. B. Schulz and J. H. Matsinger, "Rayleigh wave electromechanical coupling constants," *Appl. Phys. Lett.*, vol. 20, pp. 367–369, May 1972.
[24] T. L. Szabo and A. J. Slobodnik, Jr., "The effect of diffraction on the design of acoustic surface wave devices," to be published.